UNIVERSITY OF OKLAHOMA

GRADUATE COLLEGE

NEUROIMAGING FEATURES OF ADULTS WITH AND WITHOUT AMNESTIC

MILD COGNITIVE IMPAIRMENT

A THESIS

SUBMITTED TO THE GRADUATE FACULTY

in partial fulfillment of the requirements for the

Degree of

MASTER OF SCIENCE

By

JOHNNY O'KEEFFE
Norman, Oklahoma
2017

NEUROIMAGING FEATURES OF ADULTS WITH AND WITHOUT AMNESTIC
MILD COGNITIVE IMPAIRMENT

A THESIS APPROVED FOR THE
SCHOOL OF ELECTRICAL AND COMPUTER ENGINEERING

BY

_____
Dr. Han Yuan, Chair

_____
Dr. Lei Ding

_____
Dr. Joseph Havlicek

Acknowledgements

I would like extend my profound gratitude to my advisor, Dr. Han Yuan. I am confident that I could not have found a better advisor to work through this program alongside. Dr. Yuan taught me how to conduct responsible, ethical experiments, how to develop more sophisticated segments of code, how to express and convey my research in a professional way, and how to explore research topics in an academic manner. Time and time again, Dr. Yuan made herself available at all hours of the day and night in order to answer questions I had. Dr. Yuan spent extensive amounts of time working with me to debug code, discuss research direction, and provide encouragement and coaching for not only my research, but also my engineering career. She showed me what it means to be a successful biomedical engineer, and my greatest career goal is to become as well versed in my work as she is in hers. It was with her patience, support, and teaching that I have been able to complete this thesis work.

I would like to thank my committee members, Dr. Lei Ding and Dr. Joseph Havlicek, for their support and teachings throughout my engineering career. Both of these remarkable instructors developed my understanding of signal processing through their teaching, and I would not have been able to complete my work without their instruction.

I would like to thank my dear friends for their support throughout my Bachelor's and Master's education. Their company, lending ear, and kind words continue to drive me to be a better engineer, and I will prove to them that their faith in me is not misplaced.

Table of Contents

List of Tables

List of Figures

Abstract

Amnestic Mild Cognitive Impairment (aMCI), a condition in which the memory functions of cognition are significantly impaired, is an established risk factor for Alzheimer's Dementia, a neurodegenerative disease that has no known cure. Electroencephalography's (EEG) capability to measure the dynamics of the brain's neuronal networks makes it a powerful tool for analyzing and understanding aMCI.

In this study, I examined the brain activation patterns of four healthy subjects with those of thirteen aMCI diagnosed subjects during a one-hour afternoon sleep session by employing a 64-channel EEG data collection system. The power spectrum was analyzed to identify sleep stages, while spectral topography and source imaging techniques were employed to study the fluctuating patterns of the brain. Results of this study show distinct structures of the resting state patterns for aMCI subjects when compared to healthy controls. Furthermore, I compared the neuroimaging features from EEG to the neurological assessment of memory and additional cognitive measures in aMCI subjects. Results for source imaging analysis indicate a significant difference in the default mode network connectivities between more impaired versus less impaired aMCI diagnosed subjects. The results indicate that spatial topographies and electrophysiological networks measured by EEG may be used to characterize the neurological correlates of cognitive impairment in aMCI.

In conclusion, this proof-of-concept study suggests that EEG may be used in place of fMRI for the evaluation of brain activations associated with aMCI and its degradation levels. This development could pave the way for cheaper, more accessible neuroimaging for subjects with aMCI.

[Chapter 1: Introduction and Background]

This chapter focuses on providing a fundamental explanation of the core concepts necessary to comprehend the research work accomplished.

[Motivation and Significance of this study]

This work focuses on attempting to identify potential biomarkers for the purpose of diagnosing, or assisting in the diagnosis of, amnestic mild cognitive impairment (aMCI). I choose aMCI because it is a significant risk factor for Alzheimer's Disease, an incurable disease. The human and socioeconomic effect of this disease is profound, the factors of which will be discussed in a later section. Identification of Alzheimer's Disease at an early stage is critical to the treatment, as the methodologies for dealing with the affliction can only slow down the effects and prolong a quality of life. Because this disease fundamentally affects the brain, identifying biomarkers for the disease has become a topic of significant interest in the neuroimaging community. However, in recent years, the majority of research done employs the use of magnetic resonance imaging (MRI) and functional magnetic resonance imaging (fMRI). This study has chosen to employ electroencephalography instead of these other colloquially used technologies due to the cheap, mobile nature of electroencephalography. If successful, the results of this work could help lead to a quick, reliable clinical methodology for identifying aMCI, at which point a subject could receive further consultation from their doctor as to treatment and mitigation efforts to prevent and slow Alzheimer's Disease.

[Mild Cognitive Impairment and Alzheimer's Dementia]

Mild cognitive impairment (MCI) in humans is a known transition state between normal aging and dementia characterized by an existing, measurable decline in

cognitive functions [1], in the absence of dementia. Amnestic MCI, where the

"amnestic" denotation refers to cognitive impairment related to memory loss, is a

known risk factor for Alzheimer's disease (AD), a neurodegenerative condition

characterized by progressive memory loss, impairment of other cognitive functions, and

widespread neuronal loss [2]. Significant progression to AD, is defined by the inability

ability to take care of one's self. Not typically cause of death, AD may lead to years of

increased dependency on others, and years of care before dying from a concurrent

disorder. In adults of age 70 and older, approximately 22% are predicted to have some

existing form of mild cognitive impairment [3]. Of those that have developed mild

cognitive impairment, 60% are anticipated to develop dementia within 2 years [4].

Early characteristics of Alzheimer's Dementia include difficulty remembering

names and events, while late stage characteristics characterize function that make the

person more dependent on others, and includes impaired judgment, disorientation,

confusion, behavioral changes, as well as difficulties in speaking, walking, and

swallowing [5]. In end-stage or severe AD, the patient is bed-ridden and reliant on

around the clock care. This, coupled with the difficulties developed in communicating,

leave the victims more vulnerable to infections such as pneumonia.

The widespread brain damage caused by Alzheimer's can be seen in brain cross

sections, as depicted below in Figure 1. Notable differences between the healthy and

unhealthy brain in Figure 1 include significant shrinkage of the brain. The earliest area

effect in AD is the hippocampus. The symptomatic and physical effects of this disease

present significant challenges in treating those afflicted, and highlight the need for

further research on the subject.
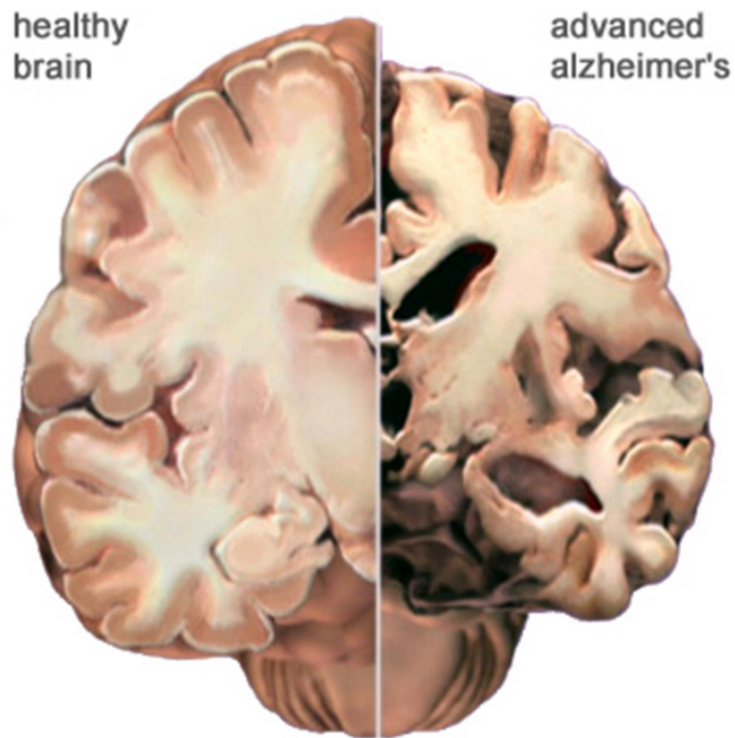
Figure 1: Healthy brain vs. diseased brain, [6]

Alzheimer's dementia has a profound human life and socioeconomic cost that simply cannot be ignored. According to the Alzheimer's Association, 700,000 Americans were estimated to have died in the year 2016 with the disease, many having died due to complications caused by it [7]. Furthermore, total payments in 2016 for health care of Alzheimer's patients were estimated to be around $236 billion. The effect of this disease not only places an emotional burden on families and friends losing their loved ones, but also forces upon them an enormous financial responsibility [7]. These socioeconomic costs and effects highlight a profound societal need for early detection, treatment, and cure for Alzheimer's Dementia.

Causes of AD are a widely studied subject. Existing studies suggest that while gene mutations may be responsible for early-onset Alzheimer's, advanced age and a

significant family history of the disease remain to be the primary causes [8]. There currently exist no known cures for Alzheimer's disease, only medications and treatments to slow the progression of symptoms [9]. Standard practices for dealing with the affliction include pharmacologic treatments such as drugs, which have a high cost associated with them, and non-pharmacologic therapies including physical therapy, mental therapy, and memory training. Non-pharmacologic therapy, while it may improve quality of life, does not slow progression of the disease, and even pharmacologic treatments are unable to grind the progression to a halt. Because of this, it is critical to develop new techniques for early detection of the disease [10].

[Sleep and Memory]

Memory processes and are well known to be disturbed in Alzheimer's disease, but the function of this phenomena is not yet understood. However, it is well known and accepted that sleep and memory are very closely related processes in the human brain, and that a decline in sleep adversely affects memory function and capability.

While even memory processes are not completely understood in the human brain, the mechanisms may be broken into three distinct events that must occur for a memory to be formed. The first event, acquisition, refers to the exposure of some information. The second event, labeled consolidation, is the process by which the brain stabilizes a memory. Finally, the last event is referred to as recall, the process by which a person is able to access a stored memory. While acquisition and recall take place almost exclusively through wakefulness, research in the field suggests that memory consolidation takes place during sleep [11].

[Electroencephalography]

Electroencephalography is a tool used for the practice of detecting and recording neural potential fluctuations projected onto the scalp. These fluctuations are detected by electrodes places across the scalp. Many modern EEG systems employ on the order of 64 to 124 EEG electrodes spread across the scalp in order to het high density data information. An example of an electrode-scalp interface may be seen below in Figure 2.
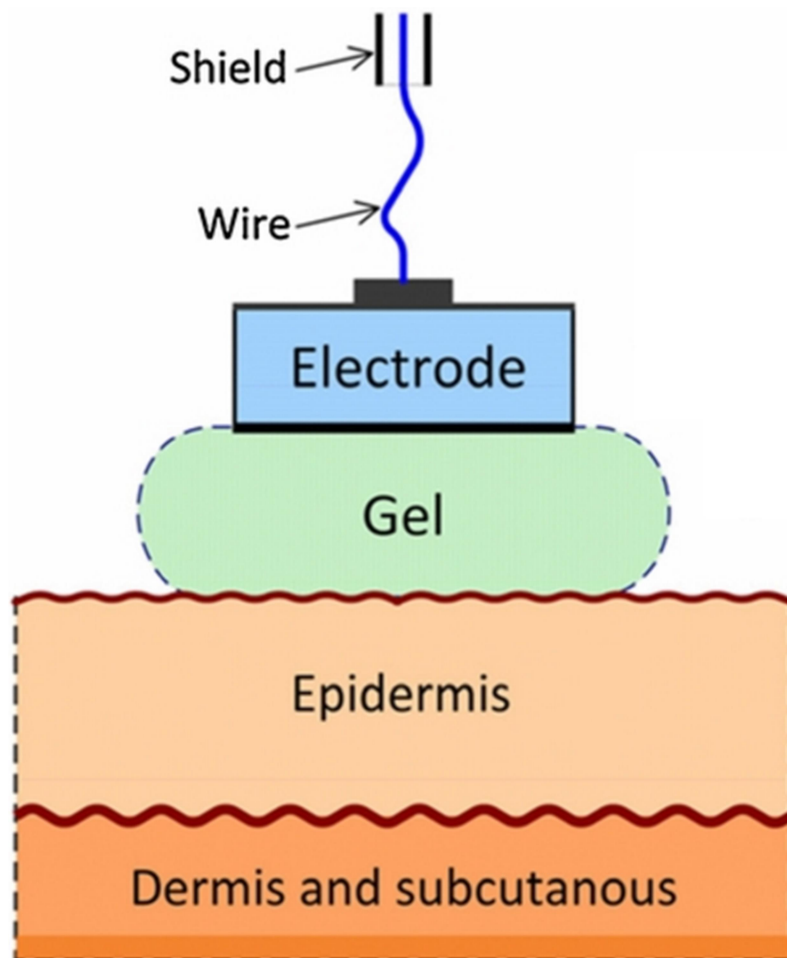
Figure 2: EEG electrode-scalp interface [26]

EEG stands out among other brain imaging modalities in that it has the combined properties of having high temporal resolution, low relative cost, and high

relative mobility [12]. This set of properties is particularly valuable because it grants EEG a high level of societal accessibility, meaning that clinics, hospitals, special treatment centers, and even mobile doctors may employ the technology across a wide range of patients and subjects.

The scalp-level fluctuations picked up by an EEG system are generated by electric fields produced by neurons that fire simultaneously in the brain. Measurement of these activities can be useful in providing insights into activity happening within the brain during different events, stimulations, and states. An example of what raw EEG data may look like can be found below in Figure 3. In Figure 3, each line of data represents an individual EEG electrode's data. In this case, the y-axis is measured in microvolts, and the x-axis measured in seconds.

Figure 3: Example EEG data

[Physiological Origins]

The study of electroencephalography begins with understanding the source of the activity. EEG measures electrical fields on the scalp of the head, which arise from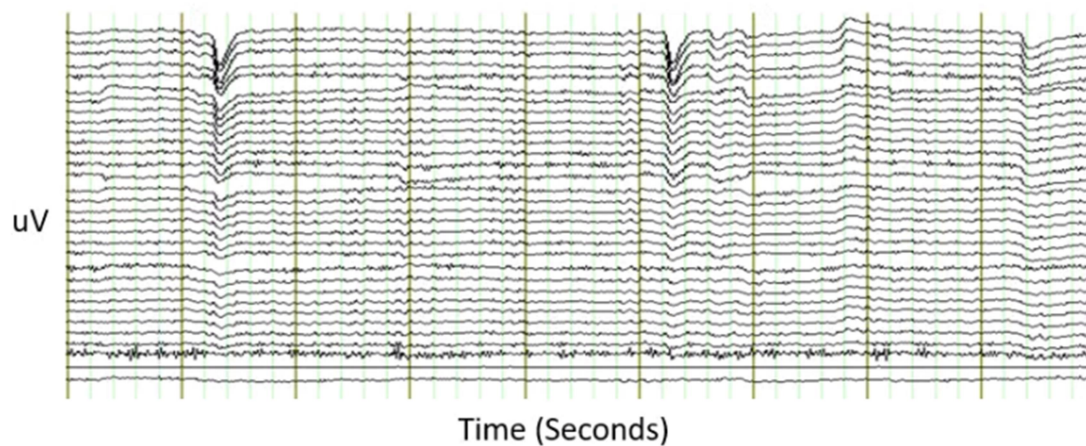 electrical activity in the brain. This electrical activity is driven by synaptic and action potentials generated by neurons. Synaptic potential, in particular, refers to the difference in voltage generated between the inside and outside of a postsynaptic neuron. When a transmitter input is received at the post-synapse, the membrane ion permeability changes and allows for a current to flow into or out of the cell. An inward flow of current results in an excitatory post-synaptic potential, while an outward flow creates an inhibitory post-synaptic potential. These synaptic processes are extremely quick to occur, but have reasonably long spatial decay coupled with relatively slow temporal decay (on the order of tens of milliseconds). Because the decay of these processes is relatively long compared to the process itself, synchronization of neural events is much more likely to be detected at the macroscopic scale.

Action potentials, however, are generated by sharp changes of the membrane potential at the soma of the neuron, which then propagates along the axon. In a converse manner to synaptic potentials, action potentials have a much quicker temporal decay, meaning it is much less likely for large levels of detectable synchronization. Additionally, these potentials are much more likely to have their electromagnetic fields cancelled out by currents occurring in opposite directions. For these reasons, the scalp-level fluctuations detected by EEG are primarily dominated by synaptic potential. These potentials may then be modeled as current dipole sources positioned perpendicular to the cortical surface at the gray matter.

[Rhythmic Activity]

Since the discovery of EEG in 1929 by Hans Berger, there has always been an acknowledged rhythmic nature present in EEG signals [13]. These rhythms have a wide spectrum, with identifiable frequencies from DC all the way to 70Hz. However, in the decades that followed the discovery of EEG, the primary focus of research with the technology focused upon event-related potentials (ERPs), the response of the brain to a specific stimulus. In these studies, the rhythmic activity of the brain was considered to be noise. In order to eliminate this "noise," ERPs were recorded hundreds of times and averaged in order to obtain the desired response signal. It has only been in recent years that the rhythmic activity has been realized to be more than simply noise in the data.

Typically, rhythmic EEG is analyzed and examined in different bands of frequencies, such as delta (0-4Hz), theta (4-8Hz), alpha (8-13Hz), beta (13-30Hz), and gamma (>30Hz) [14]. These bands of activity are known to be associated with certain tasks and actions, such as body movement, which causes a decrease in alpha frequency powers [15]. Power modulations additionally present with topographic changes in brain activities across the scalp, allowing for a visual representation of these activities to be obtained [16]. In addition to physical movement, rhythmic brain activity modulation has been recorded in response to sensory and even cognitive tasks. Oscillation is notably present across the entirety of the brain, including cerebral cortex and the subcortical regions alike. During the absence of stimuli or tasks, known as the resting state, the alpha rhythm is typically dominant, and may be seen in topographic plots as developed across the brain from a focal area in the occipital region [17]. Furthermore, such fluctuating power activations of differing frequency bands tend to show inverse

relationships. So, a decrease in low frequency band power will usually correspond with increases in higher frequency band activity [18]. An example of this is found in the transitions from wake to sleep. During the awake resting and early stages of sleep, EEG power and frequency characteristics align closely with the resting state: high alpha band activations dominating the scalp. However, as sleep deepens, high frequency power begins to diminish, and the EEG spectrum instead becomes dominated by low frequency band activities [19]. This particular example will be elaborated upon in a later section. Elucidation of the changing rhythmic patterns as a response to different stimuli, states, and tasks will serve to offer valuable insight into the fundamental functioning of the human brain.

[Source Imaging]

The focus of source imaging is aiming to determine the strength and location of the current sources which generate the potentials measured upon the scalp by EEG. However, the mathematical solution to this problem is both ill posed and non-unique, due to the fact that different configurations of sources may lead to the same measured surface distributions. Nonetheless, by introducing some a-priori assumptions mentioned below, one may retrain the problem in such a way that results in a unique, valuable solution. The result of successful source imaging is that EEG data is granted a significant increase in special resolution. This is particularly valuable when coupled with the already high resolutions in the temporal domain that is typical of EEG data collection.

Modeling the entirety of the brain's electrical activity may be approached first with the distributed current source model. This model employs thousands of current

dipoles evenly distributed around the scalp. These current dipoles may be further constrained as being perpendicular to the scalp, as the column-based organization of the neurons within the gray matter forces regional current to flow either inward or outward normal to the local cortical surface [20]. Further restraint of the current sources may be applied through the employment of anatomical information obtained through structural neuroimaging modalities, such as magnetic resonance imaging (MRI). These anatomical structural constraints may be obtained on a subject to subject basis, or they may be applied through the use of a standardized structural model.

[The Default Mode Network]

Synchronized rhythmic activities that occur across the entirety of the brain are perhaps some of the most interesting neural events. These unified responses to phenomena, or a lack thereof, are referred to as neural networks. One common network, colloquially referred to as the resting state, or default mode network (DMN), reveals the activity in the brain that occurs during rest, introspection, and general inactivity. The default mode network is characterized by co-activations between the frontal and occipital lobes of the brain. These co-activations may be seen represented in Figure 4 below.

The mapping depicted in Figure 4 is the result of fMRI imaging techniques, which measure the levels of blood oxygenation. These blood-oxygenation-level-dependent (BOLD) signals are colloquially referred to as the hemodynamic response of the brain. Historically, BOLD signals are extremely consistent across healthy subject in resting-state fMRI measurements, making them a good baseline for analysis of events which modulate this signal. However, a fundamental flaw of this measurement is that it

is an indirect measurement of neuronal activity, and is thus not fully understood. EEG

signals simultaneously acquired with fMRI data display patterns that appear to overlap.

While these two signals are starkly contrasted in their temporal resolutions, their

overlap sets the ground plane for examination of high resolution EEG as a substitute
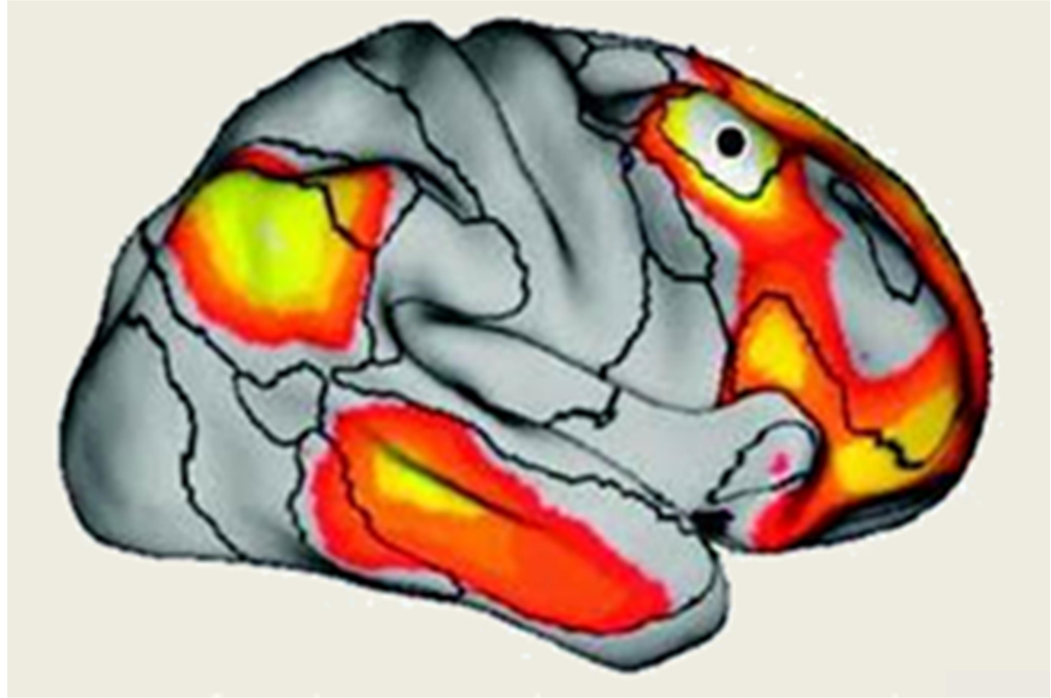
measurement [28].

Figure 4: Default mode network [21]

The default mode network is known to be altered in a variety of brain-related

illnesses including autism and schizophrenia. These disease related alterations point to a

significant relationship between brain health and the resting state network. Additionally,

previous studies and work have suggested a significant correlation between this network

and memory processing and Alzheimer's Dementia. These relationships encourage and

reinforce the study of the DMN and how it changes underneath different conditions.

[Scope]

The focus of my thesis work is to examine and identify neuroimaging features that could be used to answer the following questions:

- Is it possible to use EEG to identify differences between healthy and diseased subjects?

- Is it possible to use EEG to identify differences between diseased subjects that are more degraded versus less degraded?

These questions were explored through analysis of electroencephalography topography plots, power spectrum density plots, source imaging, and template correlation analysis.

[Chapter 2: Methodology]

This chapter focuses on outlining the study design, inclusion and exclusion criteria, experiment methodology, and strategy for processing data.

[Demographics and Exclusion]

Study procedures were approved by the local institutional review board at The University of Oklahoma Health Sciences Center. Screened subjects were excluded from the study if they had any of the following: A major neurological or neuropsychiatric condition, anticholinergics or general anesthesia in the past 6 months, conditions that would complicate the interpretation of EEG, conditions contraindicative of MRI scan, a sleep disorder, or pregnancy. These criteria were included both to ensure the safety of all subjects included as well as to ensure quality of collected data.

The study design considered three groups of subjects, individuals diagnosed with amnestic mild cognitive impairment (aMCI), aMCI who returned for a repeated visit one year afterwards, and healthy controls (HC). Upon completion of my thesis, seventeen individuals diagnosed with aMCI were recruited in the study. Among them, two aMCI individuals did not complete the entire data collection procedures, two aMCI individuals' data were discarded due to device failure or severe quality issues and one aMCI individual data was not able to fall asleep thereby the EEG data was excluded from further analysis. Three of the seventeen aMCI individuals were recruited for repeated visits. For one of the return aMCI, the data from initial visit was excluded and the data of return visit was re-grouped as aMCI. Four healthy control individuals were recruited and completed the study.

As a result, thirteen aMCI and four HC individuals had their data employed in this analysis. The demographics and the clinical assessments of the aMCI and HC study participants are listed in Table 1.

Note that the HC subjects are not perfectly age-matched to the aMCI subjects yet, which is still part of ongoing efforts. The difference in the average age is approximately 12 years. For exploratory purpose, my analyses examined EEG features for both aMCI and HC groups. In order to further study the EEG features in charaterizing the disease severity, my analyses seperated the aMCI into two sub-groups, a less impaired and a more impaired sub-group, and then examined the difference between the two sub-groups of aMCI individuals. The analysis procedures will be elaborated in the following sections. An improvement for future work could include acquiring additional subjects with better matched ages.

Table 1: Demographics of aMCI and HC

	aMCI [n=13]		HC [n=4]	
	Mean/Max possible	STD	Mean/Max possible	STD
Age	68.6	8.4	56.2	3.1
Year of Education	16.2	3.9	15	1.4
MMSE	27.3/30	2	29.5/30	0.5
CDR	0.4/1	0.2	-	-
GSD	6.4/15	1.7	0.8/15	1.3
Lawton ADL	14.1/16	1.3	16/16	0
NPI	2.1/12	0.9	1.3/12	1.3
Memory Score	10.5/36	3.1	18.8/30	8.4

Definitions of the acronyms outlined in the subject demographics figure include: HC: healthy control, MMSE: mini-mental state examination, CDR: Clinical Dementia Rating, GDS: Geriatric Depression Scale, NPI: Neuropsychiatric Inventory, Lawton IADL: Lawton Instrumental Activities of Daily Living, STD: standard deviation, n: number of subjects.

Data for this study was collected over the course of a single session per subject. EEG was captured by employing a 64-channel Brain Vision (BrainProducts, Munich, Germany) EEG system. An image of the setup, as well as an example scalp map of electrode locations can be seen below in Figures 5 and 6. Using this, data was recorded at a sampling frequency of 500 Hz, and at a sensitivity of $1\mu V$. This sampling frequency and voltage sensitivity is known to be well above the necessary sampling rate and sensitivity to acquire clean signal reconstruction.

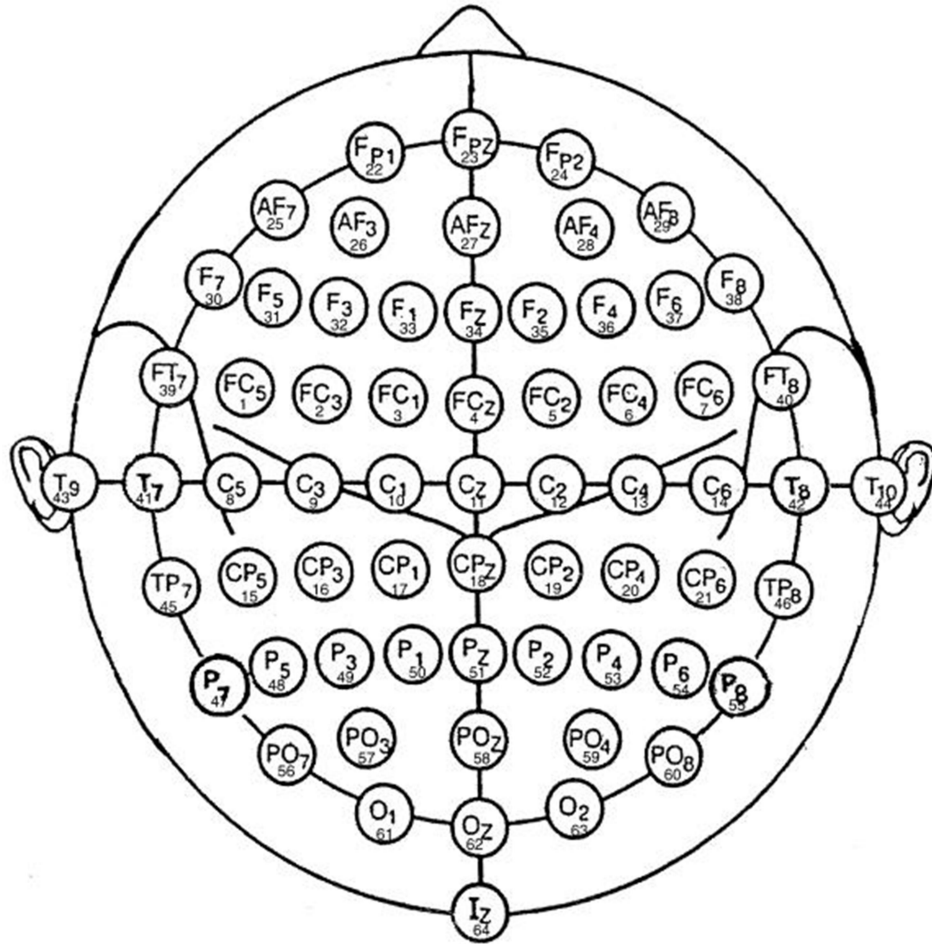**Figure 5: Image of experimental setup**

Figure 6: Example 64-channel EEG scalp map [22]

Subjects were first asked to take part in a memory encoding and free recall task outlined in Wenger et. al [27]. The encoding section involves displaying three simple items, such as boat, bike, or cherry, alongside simple cued that correlate to one of the items, such as "fruit." The subjects were then asked to point out and say the name of the item that corresponds to the cues given. This was repeated for 36 items. After the encoding session is finished, the subjects were asked to recall, freely, as many of the items as they can. The total number of recalled items was recorded and labeled as the pre-nap recall number. Examples of the items to be recalled may be seen below in Figure 7.

Item	Cues		Item	Cues	
	Category	Instance		Category	Instance
Book	Reading material	Chapter	Mountain	Earth formation	Climb
Car	Vehicle	Dashboard	Dog	Domestic animal	Pet
Shirt	Clothing	Collar	Bed	Furniture	Sheets
Pot	Kitchen tool	Copper	Heart	Part of body	Artery
Church	Type of building	Chapel	Ring	Type of jewelry	Pearl
Ball	Type of toy	Soccer	Window	Part of building	Shutter
Gun	Weapon	Trigger	Cherry	Fruit	Strawberry
Piano	Keyboard instrument	Organ	Stove	Major appliance	Range
Shoe	Footwear	Lace	Bread	Type of food	Butter
Eye	Part of the face	Sight	Cow	Farm animal	Herd
Trumpet	Brass instrument	Trombone	Knife	Eating utensil	Fork
Fly	Insect	Spider	Pencil	Writing implement	Lead

Figure 7: Example memory items, images, and cues [27]

Subjects were then asked to sit back in a recliner chair and nap for
approximately one hour for the purpose of EEG data collection. The testing room was
separated from the recording room. During the naps, the room lights were turned off
and subjects were visually monitored via a near infrared recording system. The testing
room was sound attenuated, and a white-noise machine was used to further standardize
room sound levels. Room temperatures were maintained at 68 degrees F, with blankets
and pillows provided to promote sleep. Start markers, end markers, and any activity and
movement observed during the nap via video monitor were marked in the data
recording using custom made Brain Vision event markers.

Upon completion of the nap, subjects again were asked to recall as many of the
encoded items as they were able too, freely. The total number of recalled items post nap
is used as a second measure of memory capability. This is referred to as the post-nap
recall number. The differential of items recalled after and before the nap may also be

examined in relation to sleep. The final step of this experimental procedure is a cued-recall session, in which the items that the subject did not remember after the nap are attempted to be recovered through the use of similar cues that were used to encode them. However, these cued-recall numbers were not employed for this study.
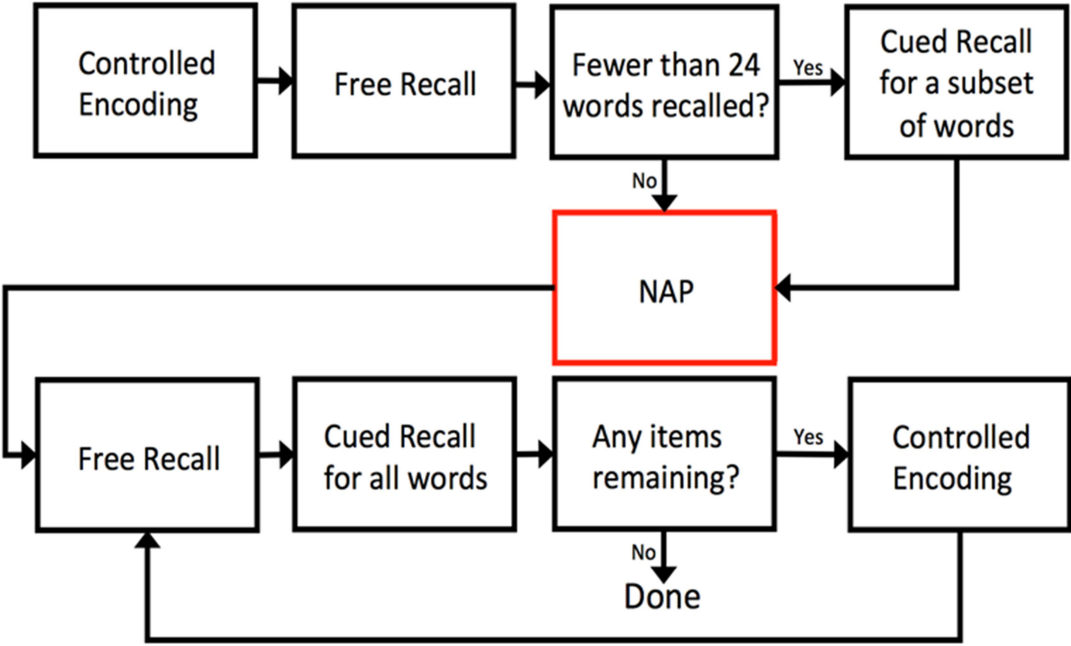
Figure 8: Experiment flowchart

[Data Preprocessing]

The entire data processing pipeline can be seen below in Figure 9. This figure depicts how the pre-processing steps flow into the data analysis.

EEG preprocessing steps are necessary to improve the signal to noise ratio of collected data. While the hardware used for data collection contains a notch filter to eliminate 60 Hz noise, as well as a low pass filter with a high cutoff of 250 Hz, this alone is insufficient to provide clean EEG.

19
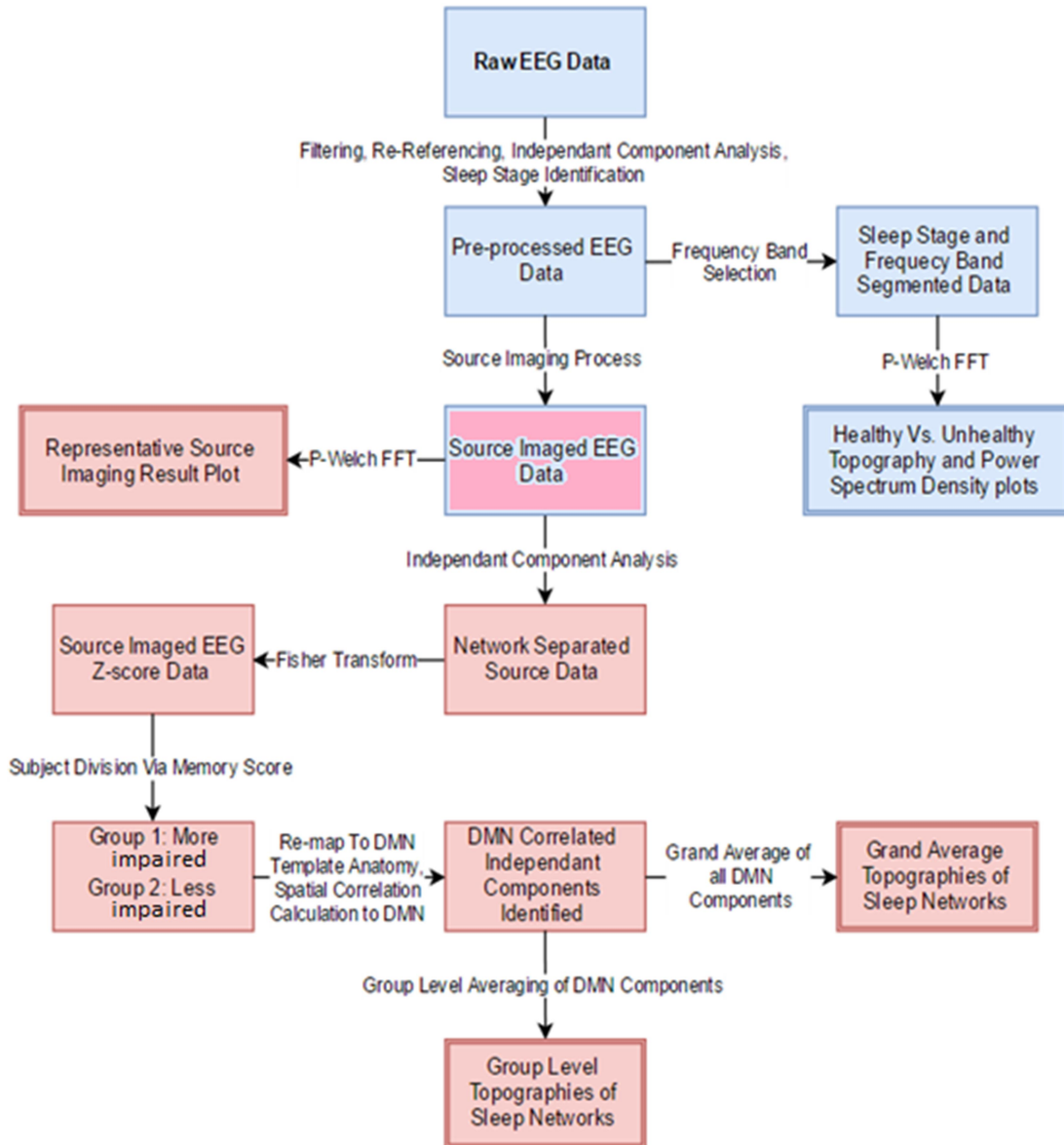
Figure 9: Data processing flowchart

The data was initially segmented by start and end markers set by the E-Prime software. Next, channels having poor impedance and contamination from muscle movements were removed. Poor impedances and muscle movement contamination in EEG data may be identified by unusually high or low frequency patterns in a given channel when compared to all other channels of data. In the remaining channels, data

segments with excessive movement artifacts were further discarded, which accounted

for less than 1% of the total data. These artifacts are easily identified as brief, high

frequency, high amplitude blasts in the data.

Following rejection, the data were processed by a bandpass filter, with a high

cutoff frequency of 100 Hz and a low cutoff frequency of 1Hz, as well as a second

notch filter at 60 Hz to further eliminate environmental effects. The filtered data then

were re-referenced by the common average referencing technique, and down sampled to

250 Hz. All preprocessing steps up to this point were conducted through the use of

BrainVision Analyzer software (Brain Products, Gilching, Germany).

Further de-noising was done using independent component analysis (ICA) via

the EEGLAB toolbox (Swartz Center for Computational Neuroscience, San Diego,

CA). ICA is a computational statistical technique employed to decompose a single

signal, composed of many different inputs, into multiple non-Gaussian signals.

Assumptions involved in this process include the assumption that the subcomponents

are non-Gaussian, and that they are statistically independent from one another. This

allows for identification and separation of different signal components and how

significantly those components contribute to the measured signal. Components with

lower numbered denotations, such as independent component 1, will contribute most

heavily to the system. A higher number denotation implies a less significant

contribution. A total of 45 to 50 independent components were examined alongside

their power spectrum plots, varying from subject to subject. While there is no current

generally accepted methodology for choosing a given number of independent

components for analysis, previous studies and work suggest that a quantity between 20

and 50 is appropriate, with more components correlating to an increase in the likelihood of the ICA process converging upon a solution. Visual inspection of components and their spectral power plots led to elimination of any residual heart, muscle, and eye related artifacts.
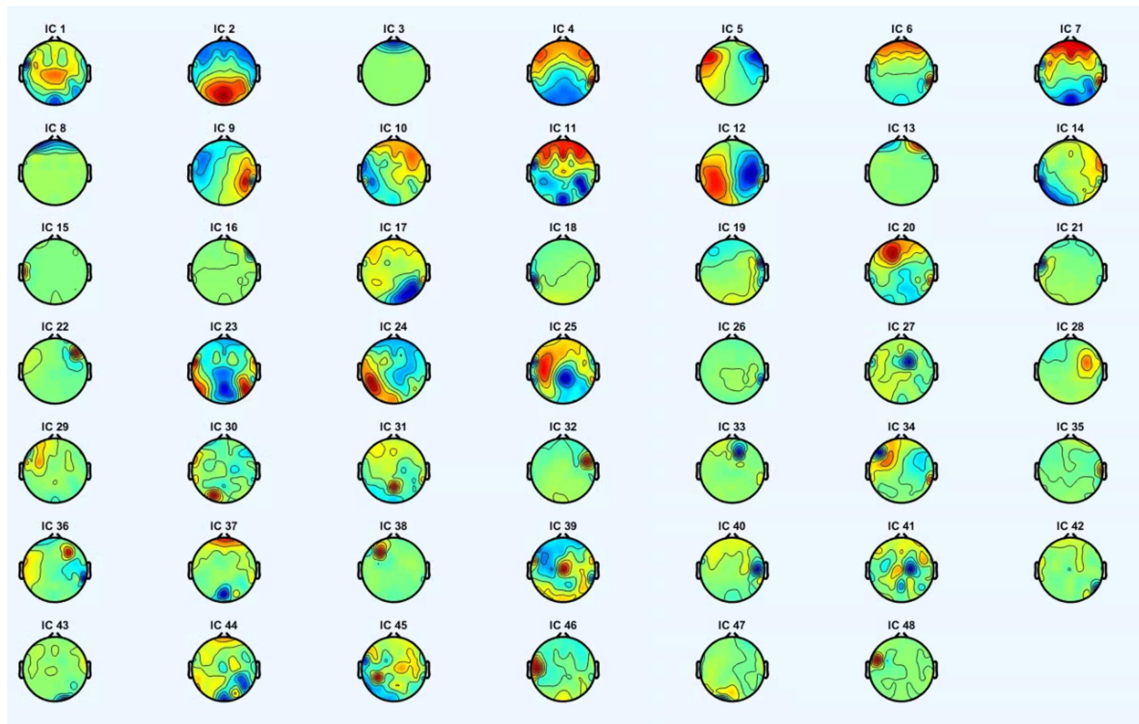
Figure 10: Example result of topographic plots from independent component analysis

Figure 10 above depicts a representative result from plotting topographic results of the ICA process. Above each scalp map is the IC number, representing its weight of signal contribution. In this example, IC number three represents what a typical eye-movement artifact may look like. Eye movement artifacts are almost always present in EEG data, and ICA is one of the best ways to eliminate this contamination. Another type of artefactual component is IC number 15, where the activity is completely

dominated by one "hole" of activity. This may be the result of muscular movements or the so-called "pop" artifacts that may arise from individual channels.
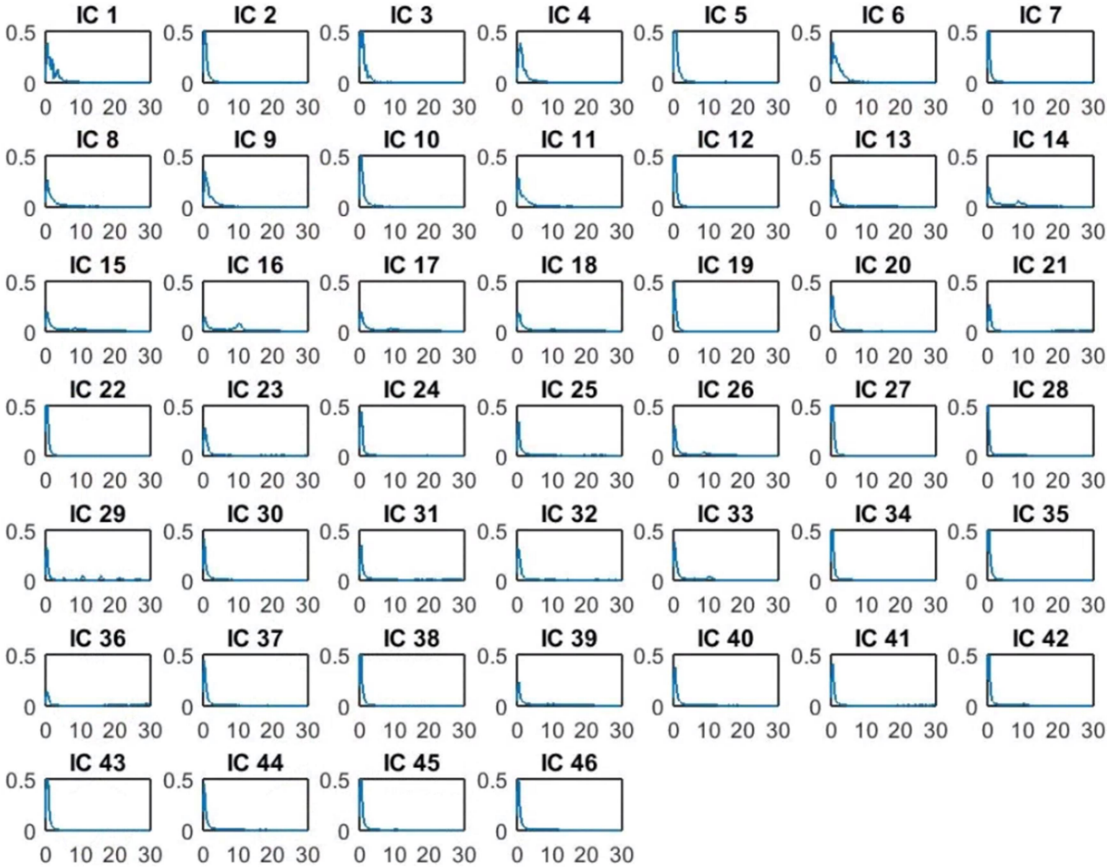
Figure 11: Power spectral density plots resulting from ICA

Figure 11 above depicts the power spectral density plots from a different representative subject than the one depicted in the previous Figure 10. This subject's plots were chosen instead to show additional criterion used for IC rejection. In this Figure, IC 6 displays a pattern typical of ocular artifact. IC 29 displays spiking in higher frequency regions, indicating contamination of this IC as well. Details outlining the methodology for obtaining the power spectrum density plots will be discussed in a later section.

With these preprocessing steps completed, the EEG data is cleaned of measurement noise, environmental noise (such as 60 Hz interference), and physiological noise of all types.

[Sleep Stage Segmentation]

The nap recordings were scored by a certified sleep clinical researcher, using the standard rules set by the American Academy of Sleep Medicine. Thirty second epochs of data were visually scored by state: either wakefulness, one of the four stages of Non-Rapid Eye Movement (Stage 1-3 NREM) Sleep, or Rapid Eye Movement (REM) Sleep.

Representative epochs of each stage of sleep were scored digitally through the analysis of the power spectrum of the signals. That is, representative EEG channels were selected, and their frequencies analyzed to determine the sleep stage during each thirty second epoch. These individually scored epochs are employed later both for individual sleep stage EEG analysis and grand averaging of sleep EEG across subjects.

[Power Spectrum and Scalp Topographies]

Power spectral density (PSD) plots for these datasets are generated using Welch's method of power estimation. This technique allows for analysis of dominant frequency activations which occur in a given set of data. The parameters used for Welch's method include a 250Hz sampling frequency, a hamming window size of 1000, and an overlap of 125.

Scalp level topographies are useful for visual representation and analysis of EEG data. In particular, this is valuable for representing results of group level averaging of data, as well as for selection of independent components that will be rejected due to artifact contamination, as presented above in Figure 10. These topographic plots are

generated using EEGLAB functions, and require both recorded data as well as channel location data in order to accurately depict the activations. Channel location data refers to the three-dimensional coordinates in space that detail where each channel is relative to one another.

[Source Imaging]

In order to improve the spatial resolution of EEG data, a technique called source imaging was employed. Source imaging employs anatomical information collected through the use of MRI, or through the use of standard MRI structural images, in order to solve the so-called inverse problem. This inverse problem, a fundamentally ill-posed problem, is a matter of solving for the distribution of the dipole strengths within the brain based on recorded data. By solving this problem and obtaining a unique solution, one may determine the sources of EEG activity from a 3D distribution of neuronal activity. Equations that describe this process include

$$\Phi = A \bullet S + N. \tag{1}$$

where Φ is a matrix of the measured EEG, S is the unknown matrix of amplitudes of the source dipoles in time, A is the mixing matrix, and N is a vector specifying the noise at each electrode. Source estimation was achieved by using a minimum norm method to derive the linear inverse operator expressed by

$$W = RA^T (ARA^T + C)^{-1}. \tag{2}$$

for which C and R are covariance matrices of the noise and sources, respectively.

In this analysis, I employ an L-2 minimum norm methodology for solving the inverse problem, as outlined in the equations above as well as in in [23, 28]. This technique corresponds to the 3D distribution of current densities of dipole sources on

25

the cortical surface with maximum levels of similarity, in terms of orientation as well as strength, between neighboring neuron groupings. Because anatomical structural MRI data was not available for all subjects involved in our study, I employed a standardized brain model. The result of our source imaging technique is that the spatial resolution of our EEG data is refined to the millimeter level, rather than the centimeter level. For sleep stage analysis, forty second epochs of each stage for each subject were selected in order to reduce the processing strain of the source calculations.

[Template Matching]

In order to obtain a quantitative measure with which to analyze the data, I calculated a correlation between the source imaging results and a template of the default mode network. However, this problem is complex, as the measurement of EEG is not network selective. This means that our EEG data records all networks active in the brain, including the default mode network as well as many others. While the process of independent component analysis enables us to identify and separate out different networks, it is possible to have multiple networks identified which resemble the default mode network. An additional complication is developed due to the fact that ICA result weights are not the same from subject to subject. For example, the weight of independent component five for subject one may not have the same value as the weight of subject two's independent component five.

In order to address the issue of unequal weights, the source image data undergoes a fisher transformation to convert all data points into z-scores. This changes all data to fall within values from negative one to positive one, regardless of their

original ranges. With new equal weighting across subjects, averaging and direct comparisons from subject to subject is possible to conduct.

With the data of equal weight available for use, the following step is to compare to a default mode network template. However, our source image data suffered from being mapped to a different anatomical structure than our template. In order to properly conduct calculations between the data and template, the z-scores were re-mapped onto the same anatomical structure as the template.

Lastly, the process of determining the best match of independent component to default mode network was comprised of calculating the spatial correlation coefficient between the re-mapped z-score data and the template. This calculation was done for each of the twenty-five independent components of the resting-state awake data in order to identify the best match.

With the best match to the default mode network determined for the awake resting state, the process of determining the best match to the default mode network for the three sleep stages would follow. In order to reduce the effect of the non-stationary property of EEG, the awake resting stage for each subject that is identified to be the best match to the DMN template is then used as that subject's new individual template for the DMN. Spatial correlation coefficients are then calculated between this new individual template and Stage 1 NREM, Stage 2 NREM, and Stage 3 NREM sleep. This process generates a set of independent components most likely to be numerically identified as the default mode network on an individualized basis. With this set of components, an evolution can be plotted to examine the change of the DMN as sleep deepens.

[Chapter 3: Results and Discussion]

This chapter will discuss both the results of the study as well as delve into discussion in sections. This structure was chosen to make chronological order of the examined components easier to discuss and refer too. The scope of this chapter focuses on two pillars of the study: Neuroimaging Features and Study of MCI. Table 2 below outlines the foci of these two pillars.

Table 2. Structure for results and discussion

Neuroimaging features	Study of MCI
Feature 1 (sensor level): topography of activation	Between group comparison (features of MCI vs.
Feature 2(sensor level): spectrum and dynamics (sleep stages)	features of Control)
Feature 3 (source level): network connectivity	Within group comparison (correlation between
Feature 4 (source level): spectrum and dynamics (sleep stages)	features of MCI and Severity degrees of MCI)

In these results, there exist two different "levels" of plots to be considered. The first level, considered to be the sensor level, is produced as a direct result of the EEG measurements produced by the electrodes. The second level, our source level, refers to plots generated as a result of the source imaging technique described previously. These levels of results are both uniquely valuable for the insights they reveal about brain activities.

[Neuroimaging Features: Sensor Level Results]

Analysis of results is best begun by examining the sensor level topographies and power spectrum densities. Figure 12 below displays the evolution of spectral topography plots as sleep deepens for the average of all aMCI diagnosed subjects. These spectral topographies are divided into three different bands of activity in an attempt to isolate and identify changes occurring in each band of frequency across

subjects. The bands in consideration for this plot are the Delta band (0Hz to 4Hz), the Theta band (4Hz – 8Hz) and the Alpha band (8Hz – 13Hz).

Figure 12 is divided not only by frequency band, but also by sleep stage. For this figure, resting awake, Stage 1 NREM, Stage 2 NREM, and Stage 3 NREM sleep are to be examined, with higher NREM Stage indicating higher thresholds of arousal and deeper levels of sleep. The top of these topography plots indicated the front of the brain (frontal), while the bottom reflects the back of the brain (occipital). Colored activations are indicators of electrical activity measured in microvolts (μV). Each band of frequency has a colorbar indicator set to a constant range for easier analysis between stages. This colorbar was not set to be equal across different frequency bands due to the significantly differing values of activation within different bands.

The first feature of note to be examined in this is the 8-12 Hz frequency band for the resting awake stage. This topography plot depicts high levels of activation in the occipital areas of the brain, a result that is well established by previous studies. Re-obtaining this standard result serves as a methodology for verification and validation that the processing methodology is functioning correctly.

The sleep evolution in Figure 12 depicts an increase in delta level activity and theta level activity as the subject slips deeper into sleep. Increases of delta band activity as sleep deepens is an expected result, as deeper levels of sleep are known to be associated with lower frequency activity in the brain. The theta band mirrors this rise in activations as sleep deepens. Lastly, the figure reveals that the alpha band does not appear to change significantly as sleep deepens for these aMCI subjects, although it is present across the scalp.
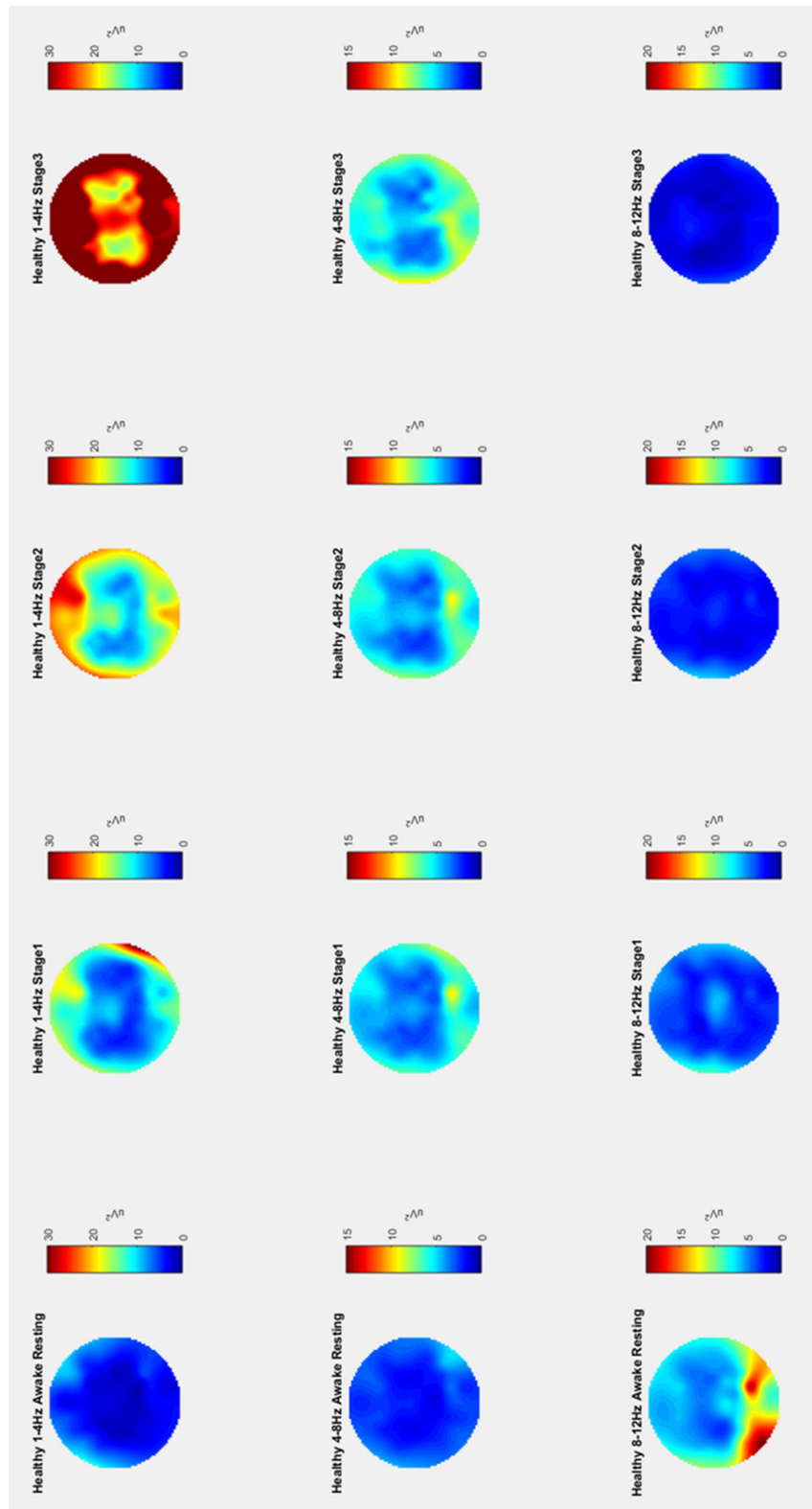
Figure 12: Average spectral topographies for aMCI subjects in Delta (1Hz - 4Hz), Theta (4Hz - 8Hz), and Alpha (8Hz - 13Hz) frequency bands
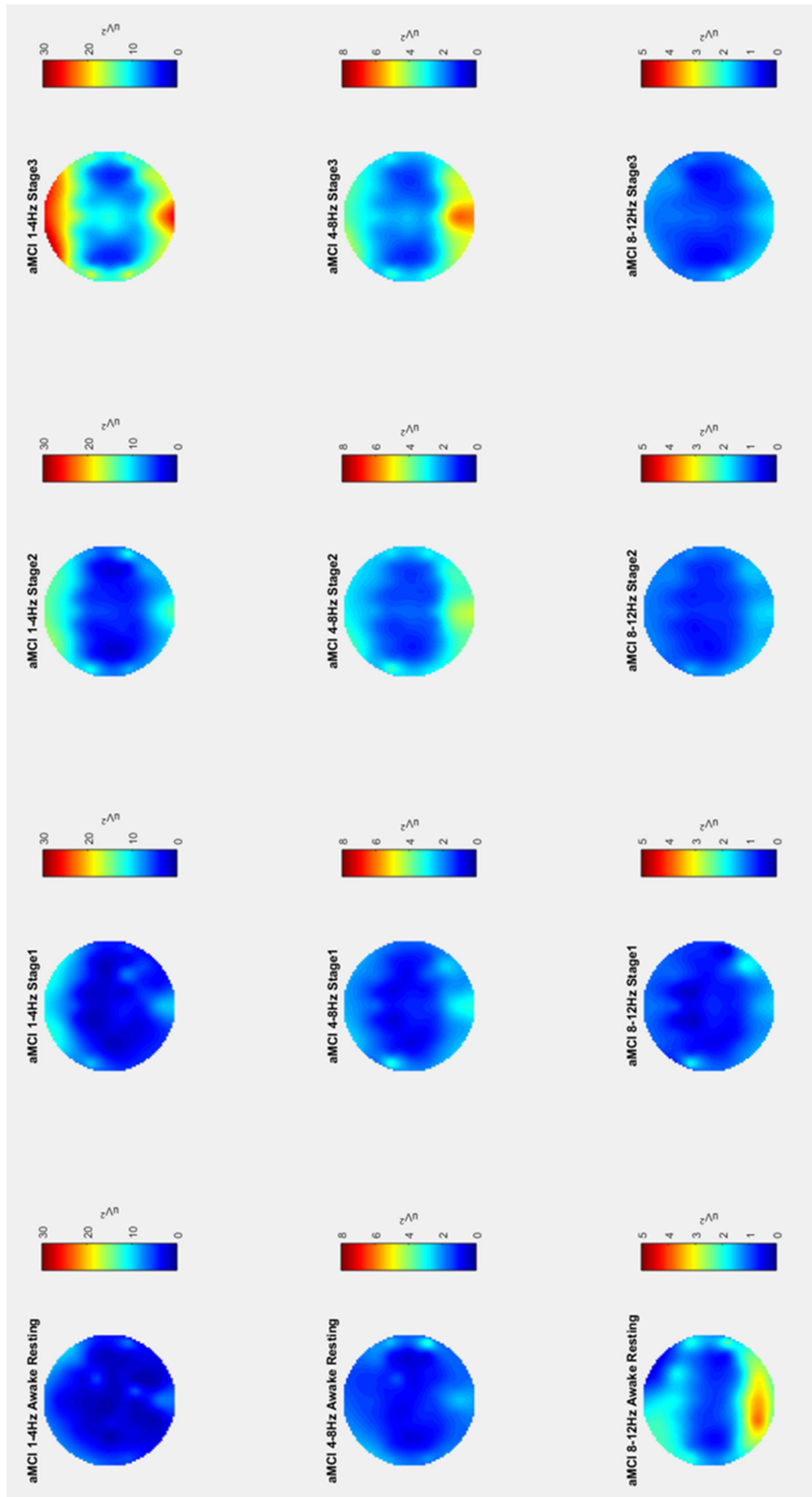
Figure 13: Average spectral topographies for Healthy subjects in Delta (1Hz - 4Hz), Theta (4Hz - 8Hz), and Alpha (8Hz - 12Hz) frequency bands

Figure 13 above indicates the spectral topography plots for healthy subjects across Alpha (8Hz -12 Hz), Theta (4Hz – 8Hz), and Delta (1Hz – 4Hz) frequency bands for Stage 1 NREM, Stage 2 NREM, and Stage 3 NREM sleep. Once again, the awake resting plot for the 8-12Hz band depicts significant levels of activity on the posterior region of the brain, validating the processing procedures. The sleep plots depict a heavy increase in delta wave activity as sleep deepens, alongside a moderate increase in theta band activity as well. These subjects, however, show little to no activity at all in the alpha band during sleep, with only a small amount of activity in stage one of sleep. Of particular interest are the patterns depicted in the Delta band for stages two and three of sleep, where activations in both the frontal and posterior areas of the brain are concurrently dominant, creating a co-activation pattern.

In addition to these topographic plots, the EEG spectra may be examined through the use of their Power Spectrum Density (PSD) plots. These figures reveal a breakdown of the dominant frequency components in the data. PSD plots typically have the y axis set to a normalized amplitude, and the x axis set to hertz. A higher normalized amplitude for any given frequency corresponds to higher domination or presence of that particular frequency in the data. Figure 14 below depicts a PSD plot for both aMCI and healthy subjects, respectively.

Figure 14: Power spectral density for aMCI subjects versus healthy subjects for electrode POz

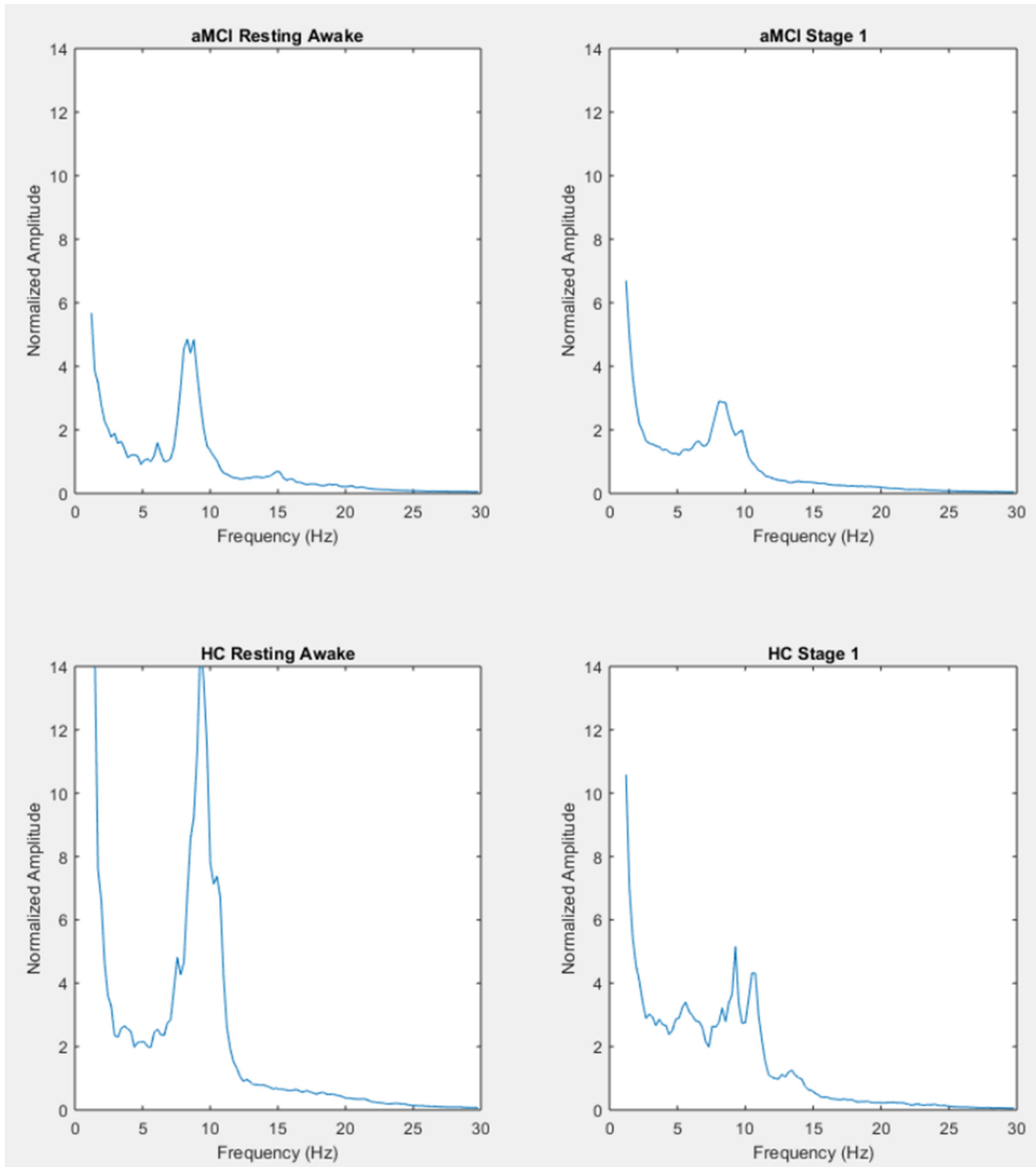This PSD figure was developed through the averaging of data collected from electrode POz for each subject in their respective groupings. POz was chosen both for its central position on the scalp, as well as for its proximity to activations of interest. The figure suggests a stark difference in the alpha band between the subject groups,

with healthy subjects exhibiting significantly higher levels of alpha band (8-12Hz) normalized amplitudes. In addition, we see a shift of dominant frequency activity as sleep deepens. While alpha band is largely evident in the awake state for both groups, this band becomes less dominant as the subjects enter sleep, with lower frequency bands becoming more dominant as sleep deepens.

[Neuroimaging Features: Sensor Level Discussion]

Comparing healthy sensor level plots to diseased sensor level plots reveals several distinct feature differences in both the topographic plots as well as the power spectrum density plots. To discuss and compare the results in the order they appear, the first topic is the delta band topographic activities.

Healthy subject delta topographies present as high-powered activations around and across the scalp, increasing in presence as sleep deepens. These plots are characterized by patterns of activity in the frontal, temporal, and posterior areas of the brain, creating a "ring" of dense activity around the scalp map, the most prominent rings presenting in stage three sleep. In contrast, diseased subjects do not generate the same powerful "rings" in the delta band. aMCI subjects exhibit activations only in the frontal and posterior regions of the brain, and at activations levels lower than their healthy counterparts. Activations in this frequency band are expected to rise as sleep deepens, making the delta band one of the most synonymous with healthy sleep patterns. Decreases in activation levels alongside reduced areas of activation for unhealthy subjects suggest that their sleep is indeed being affected adversely.

Moving onto the theta band activations, the healthy subjects and the diseased subjects begin to show more similar patterns of activations, with both groups showing dominant activities in the frontal and posterior lobes. However, a still notable difference between the groups is a lower activation power for the diseased subjects. The lower levels of theta band activations in the unhealthy subject group may be a result that makes sense, as this band is strongly associated with memory processes [24]

Lastly, the alpha band depicts strong levels of activation in the posterior region for both healthy and unhealthy subjects in the awake resting state, for which the healthy subject shows higher activation powers. However, as sleep advances, both groups show a significant drop in activity in the alpha band, such that there is virtually no alpha activity in their sleep waves. These results for the alpha band are consistent with previous work done in the area of neuroimaging, and serve as a validation measure for our results. Analysis of the power spectrum plots for the healthy versus unhealthy subjects further confirms the results measured in the topography plots: overall higher levels of activation for healthy subjects. However, the power spectrum better reveals the significant difference in alpha band activations between the subjects, with the healthy group experiencing activations more than four times more powerful.

[Neuroimaging Features: Source Level Results]

In order to evaluate the differences between levels of degradation in the unhealthy subject group, a source imaging approach was chosen. This methodology was chosen to allow for re-mapping of the EEG results to a brain anatomy that matches to a template used in previous fMRI studies. Re-mapping our data to a template anatomy allows for template matching and analysis of comparative networks.

Figure 15 is a depiction of a representative subject's source imaging results. As mentioned in the methodology section, these plots are generated as a result of selecting the independent component of the awake resting state that is best matched to the default mode network template via a spatial correlation calculation. The sleep stages are then chosen as the independent components that are best matched to the awake resting state independent component.
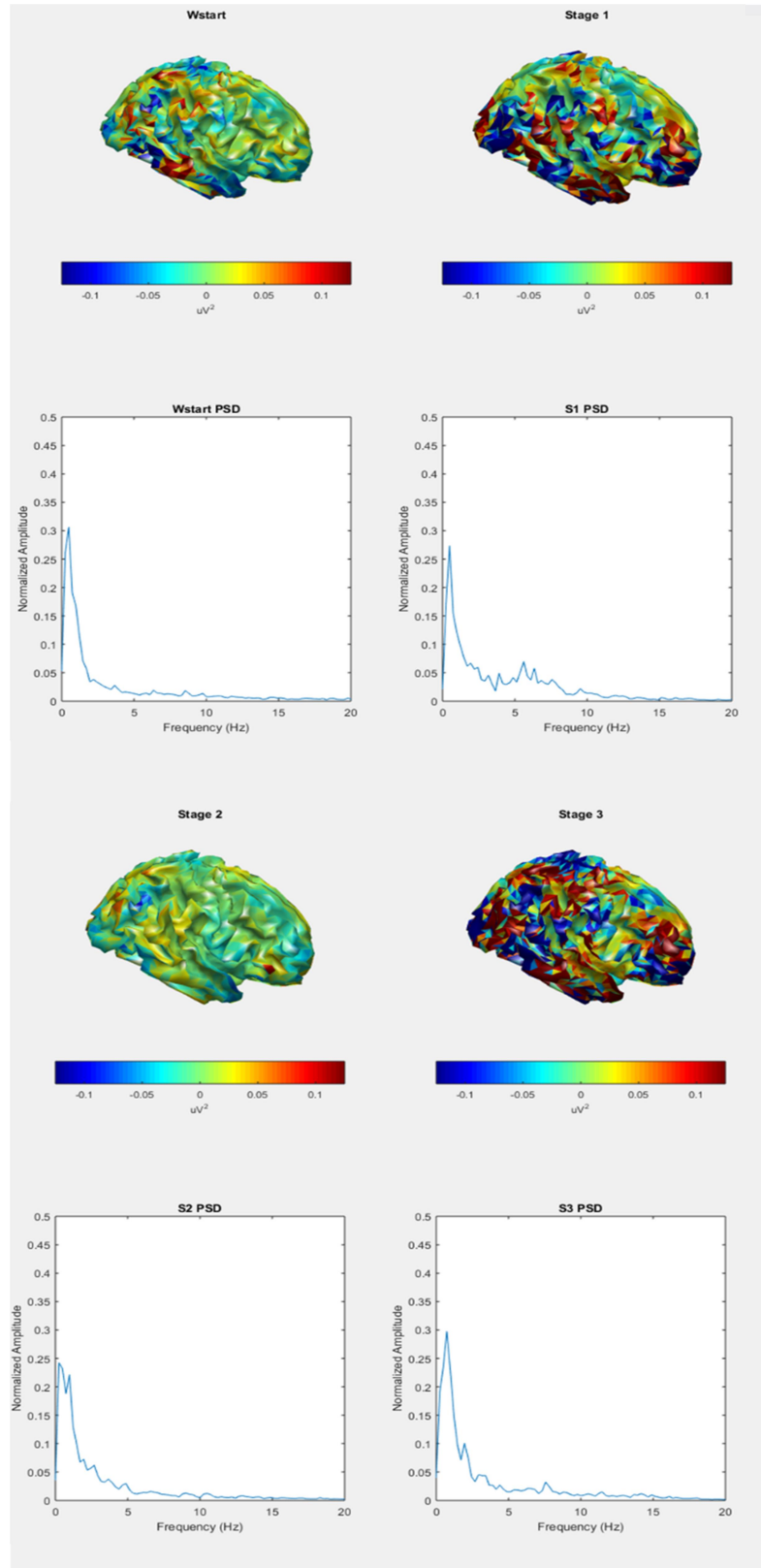
Figure 15: Representative subject source results and PSD

The result of plotting an individual subjects is, unfortunately, difficult to analyze. While it is important to maintain a consistent colorbar across stages in order to properly examine differences between subjects, doing so in this case results in stages that are either crowded by high amplitude information or devoid of region activations significant enough to visually interpret. Furthermore, the power spectrum representations of these particular independent components do not depict strongly varying frequency dominances between stages.

In an effort to obtain plots with better visual properties for analysis, group analyses were examined. Subjects were first split into two different groupings. To accomplish this, memory scores of the subject were outlined and divided. The dividing score was chosen such that the two resulting groups had similar sizes (an equal size being impossible due to the number of aMCI subjects being 13). Group 1 is defined as those who remembered fewer items in the memory task, assumed to be more impaired, and Group 2 is defined as those who remembered more items, defined as less impaired. The difference in the memory items recalled between the groups shows significance (P<0.02) in a two-tailed t-test. In addition to the two groups, plots were also developed for the combined set of subjects for comparison.

Table 3. More impaired vs. less impaired demographics

		Age	Years of Education	MMSE	CDR	GSD	Lawton ADL	NPI	Memory Score
aMCI More Impaired n = [6]	Mean	71.3	16.5	26.0	0.5	2.8	15.8	2.0	6.5
	Std Dev	7.4	2.8	1.8	0	1.9	5.1	1.5	2.8
aMCI Less Impaired n = [7]	Mean	61.6	15.0	28.4	0.4	1.6	14.3	2.3	14.0
	Std Dev	6.9	3.4	1.4	0.2	1.4	1.5	1.1	3.8
p-value		**0.03**	0.4	**0.02**	0.36	0.22	0.50	0.72	**0.002**

Conducting two-tailed t-tests between each evaluation feature of the two groups reveals significant differences in their ages (p = 0.03), MMSE scores (p = 0.02), and their memory scores (p = 0.002). These significance values highlight the differences in our two subject groups, where age and memory appear to be correlated in a way that is expected. However, there are no significant differences in years of education, CDR score, GSD, Lawton ADL, or NPI values between these subject groups, lending to their similarity in aspects other than age, mental status, and memory.
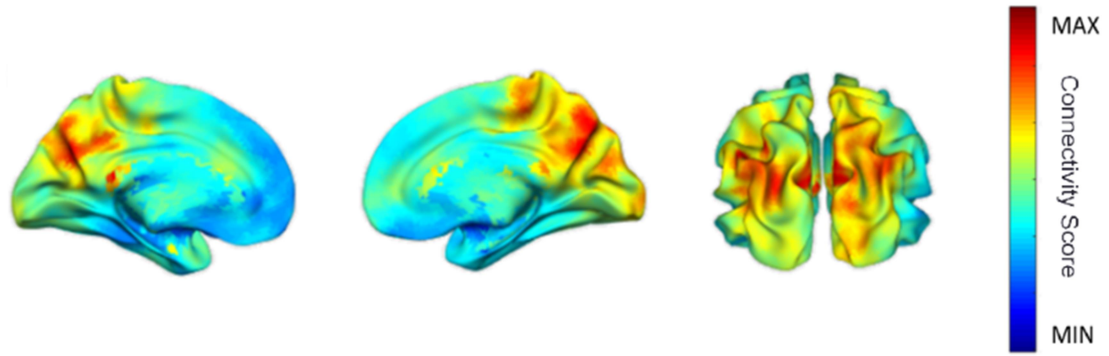
Figure 16: Sleep topography evolution averages for more impaired subjects

Figure 16 above depicts the average awake resting state topographies for the more impaired subject group. This plot demonstrates significant regions of connectivity in the posterior areas of the brain.
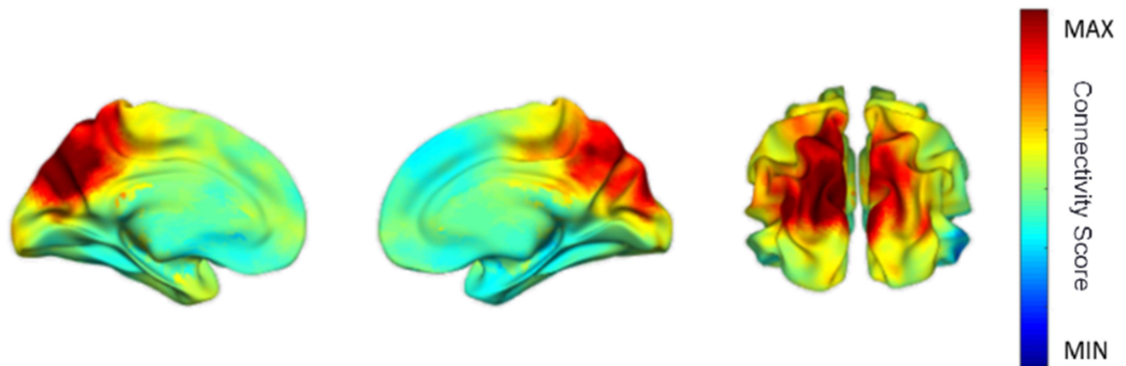
Figure 17: Sleep topography evolution averages for less impaired subjects

Figure 17 displays average topographic plots of the awake resting state for the less impaired group. These subjects also show significant regions of connectivity in the posterior regions of the brain.

In order to better examine the difference of default mode network matching between groups, side-by-side topographic plots were deemed appropriate. Figure 18

depicts the change in the topography across groups for the situation of awake resting. In particular, this figure also includes results from healthy controls for comparison.

Figure 18: Resting awake topographies across groups

Differences in the awake resting state prompted a t-test calculation between the two groups' z-score data. A plot of the t-test results in the form of brain topography may be seen below in Figure 19.

Figure 19: More impaired vs. less impaired T-test topography for awake resting state

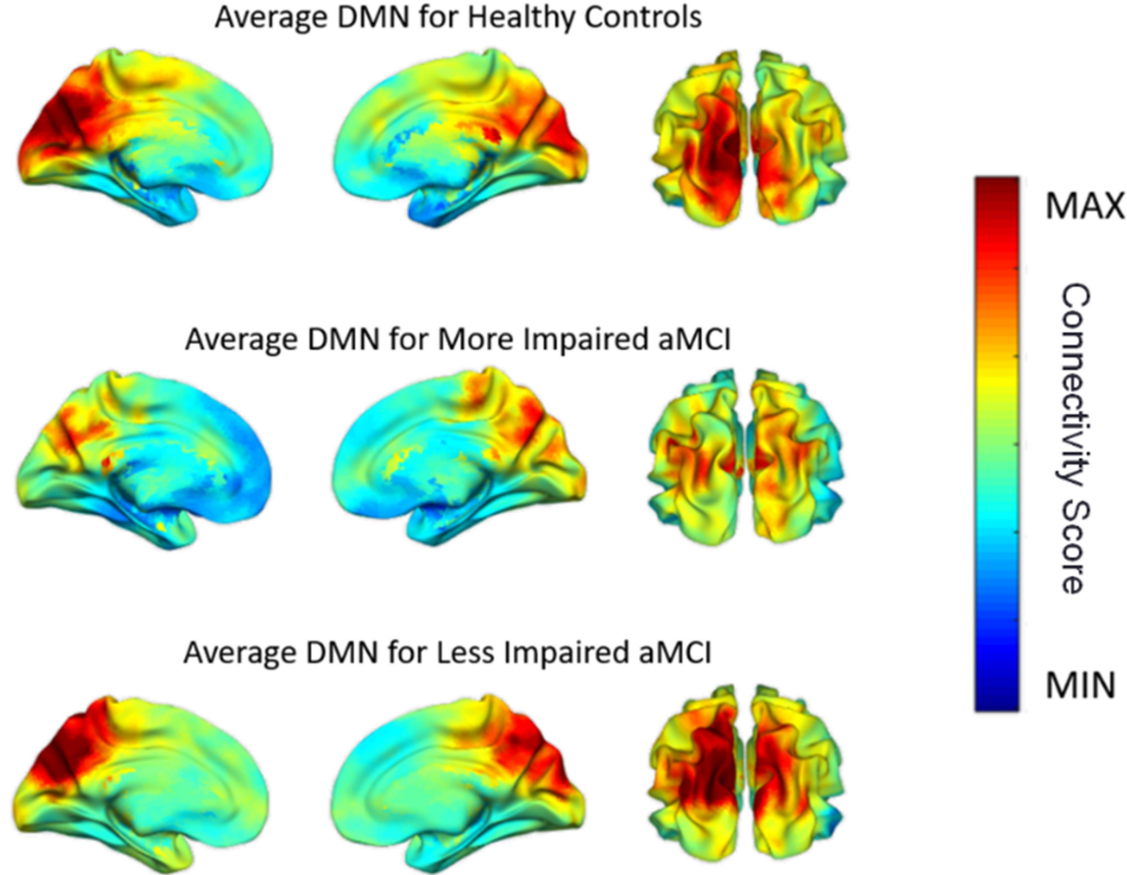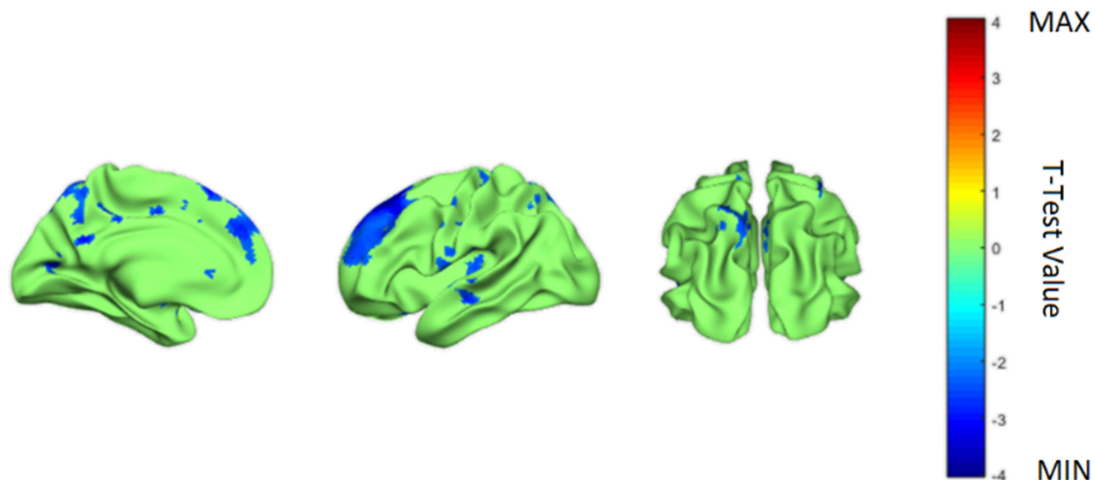The t-test topography depicts the differences between group 1 and group 2 topographies for the resting awake state. This mapping was thresholded such that only statistically significant differences ($p<0.05$) regions are plotted on the blank mapping. The blank mapping in this case is green, while regions of interest are depicted in blue. The results show significant differences in connectivity in the posterior and medial prefrontal areas of the brain.

A mask was created through the intersection of the t-test topography results and the default mode network template topography. This mask was employed to analyze the differences in the average z-scores, or connectivity scores, of the subjects as they compared to the MMSE and memory scores. However, no trend in memory or MMSE score was found when compared to these average z-scores. Statistical analysis was conducted on the average z-scores of the awake resting state default mode network for less impaired and more impaired groups and revealed that these two groups have a statistically significant difference ($P= 0.025$) in their average z-scores for the DMN.

However, it is important to note that this significance is merely a validation measure of our t-test plots. Figure 20 below delivers a visual representation of the difference of the connectivity scores between these three groups.
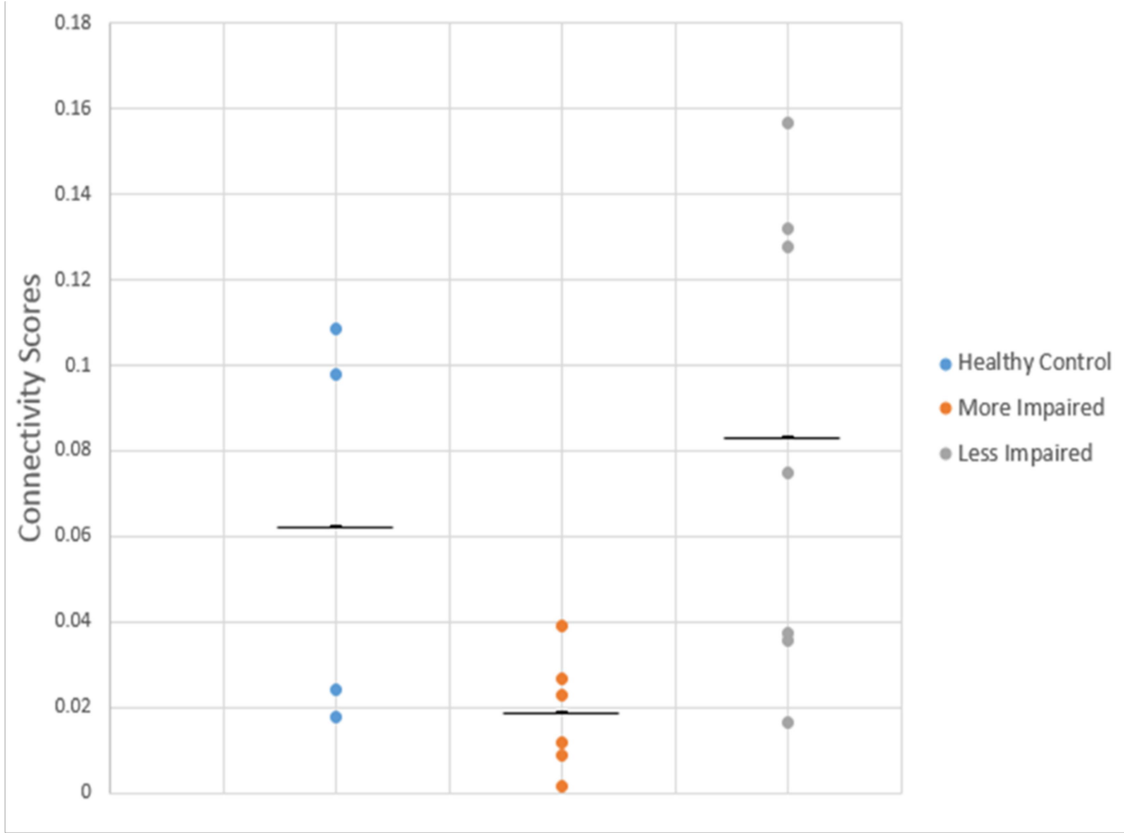
Figure 20: Connectivity scores across groups

[Neuroimaging Features: Source Level Discussion]

Topographic plots of group-level source imaging results show significant differences between the less impaired and more impaired subject groups. Visually, it can be seen that the more degraded subject group has stronger activations across the scalp than the less degraded group. Examination of the awake-resting state shows that the less impaired has connectivity patterns more prevalent in the posterior region of the brain than the more impaired group. The healthy subject group appears to have more

43

significant levels of connectivity in the DMN than the more impaired subject group, but less than the less impaired subject group.

The result of the less impaired group having stronger default mode network characteristics was surprising to the research group, but has been found to be consistent with previous fMRI studies [29]. Figure 21 below depicts the similarities between the imaging modality results.

Figure 21: fMRI vs. EEG aMCI results [29]

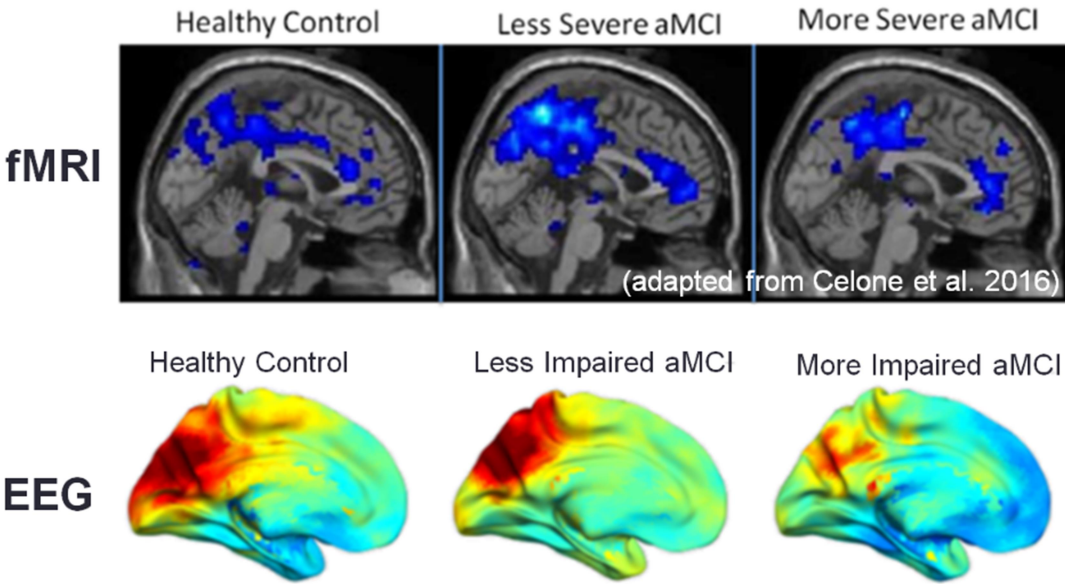The implication of the result depicted in figure 21 is that EEG source imagining may have the capability to be used as a substitute for the fMRI imaging modality.

[Chapter 4: Summary and Perspectives]

This research work has focused on EEG analysis of subjects with and without aMCI, an intermediate step between healthy functioning and Alzheimer's Disease. This research work is important because there exists no known cure for Alzheimer's Disease, only steps and measures to slow the progression. This makes early detection and identification of risk factors of the utmost importance. Identification of a biomarker to detect or assist in the diagnosis of aMCI would allow subjects and doctors to better evaluate what steps may be necessary to protect their brain's health.

Our first focus, the sensor level evaluation of EEG, revealed that our aMCI subjects have stark differences in their scalp activation topographies as well as in their power spectrum density plots. Their differences were most significant in the delta and theta frequency bands, where unhealthy subjects had significantly reduced activations. These band activations, associated with sleep and memory respectively, suggest that the disease affects both memory and sleep quality. Whether or not the sleep quality is the driving factor for the memory issues, however, remains to be explored.

Analysis of the source level results first began with a focus on analysis of development of sleep stages between different levels of degradation into aMCI. However, as these results developed further and further, promising results were instead found strictly in the awake-resting state. There, I found statistically significant differences in the connectivities of the default mode network to the awake resting state between less impaired versus more impaired subject groups. The most interesting result, however, lies in the fact that our EEG source imaging results match very closely with

results gathered using fMRI. This development suggests that source imaging has some of the same network identifying capabilities as fMRI.

In conclusion, this proof-of-concept study has proven that EEG may have the potential to be used in place of fMRI for the evaluation of brain activations associated with aMCI and its degradation levels. This development could pave the way for cheaper, more accessible neuroimaging for subjects with aMCI.

[Chapter 5: Products of This Work]

In addition to the work conducted as outlined in this thesis, I also prepared abstracts, papers, and presentations to present my work to the academic community. These products include:

- Journal manuscript in preparation

    - **O'Keeffe J**, Carlson BW, De Stefano L, Wenger MJ, Craft MA, Hershey LA, Hughes J, Wu D, Ding L, Yuan H: Alterations in default mode network in amnestic mild cognitive impairment: an electroencephalogram study. To be submitted to *Journal of Neural Engineering.*

- Published Proceedings

    - **O'Keeffe J**, Carlson BW, De Stefano L, Wenger MJ, Craft MA, Hershey LA, Hughes J, Wu D, Ding L, Yuan H: EEG fluctuations of wake and sleep in mild cognitive impairment. *39th Annual International Conference of the IEEE Engineering in Medicine and Biology Society*, Jeju Island, Korea, 2017. **[oral presentation]**

    - Chen Y, Farrand J, Tang J, Chen Y, **O'Keeffe J**, Shou G, Ding L, Yuan H[*]: Relationship between Amplitude of Resting-State fNIRS Global Signal and EEG Vigilance Measures. *39th Annual International Conference of the IEEE Engineering in Medicine and Biology Society*, Jeju Island, Korea, 2017. [poster]

- Published Abstracts

    - **O'Keeffe J**, Carlson BW, De Stefano L, Wenger MJ, Craft MA, Hershey LA, Hughes J, Wu D, Ding L, Yuan H*****: EEG fluctuations of wakefulness and sleep in mild cognitive impairment. *23rd Annual Meeting of the Organization for Human Brain Mapping*, Vancouver, Canada, 2017. [poster]

    - Chen Y, Farrand J, Tang J, Chen Y, **O'Keeffe J**, Shou G, Ding L, Yuan H: Amplitude of resting-state fNIRS global signal is related to EEG vigilance measures. *8th International IEEE EMBS Neural Engineering Conference*, Shang Hai, China, 2017. [poster]

    - Farrand J, Chen Y, Tang J, Chen Y, **O'Keeffe J**, Shou G, Ding L, Yuan H: Multimodal imaging of human brain auditory responses using simultaneous EEG and fNIRS. *1st OU-OUHSC Biomedical Engineering Symposium*, Oklahoma City, OK, 2017. [poster]

References

[1] R. Petersen, "Mild Cognitive Impairment", New England Journal of Medicine, vol. 364, no. 23, pp. 2227-2234, 2011.

[2] H. Querfurth and F. LaFerla, "Alzheimer's Disease", New England Journal of Medicine, vol. 362, no. 4, pp. 329-344, 2010.

[3] Plassman BL, Langa KM, McCammon RJ, et al. "Incidence of dementia and cognitive impairment, not dementia in the United States", Annals of neurology, vol. 70 no. 3, pp. 418- 426, Sep 2011.

[4] Brookmeyer R, Evans DA, Hebert L, et al. "National estimates of the prevalence of Alzheimer's disease in the United States. Alzheimer's & dementia", Alzheimer's Association, vol. 7, no. 1, pp. 61-73, Jan 2011.

[5] "2016 Alzheimer's disease facts and figures", Alzheimer's & Dementia, vol. 12, no. 4, pp. 459-509, 2016.

[6] "Healthy vs. Alzheimer's", Alz.org, 2017. [Online]. Available: http://www.alz.org/braintour/healthy_vs_alzheimers.asp. 2017.

[7] "2016 Alzheimer's disease facts and figures", Alzheimer's & Dementia, vol. 12, no. 4, pp. 459-509, 2016.

[8] Munoz DG, Feldman H. "Causes of Alzheimer's disease", CMAJ , vol. 162, no. 1, pp. 65-72, 2000.

[9] P. Scheltens et al, "Alzheimer's disease", The Lancet, vol. 388, pp. 505-517, 2016.

[10] E. Cavedo et al, "The Road Ahead to Cure Alzheimer's Disease: Development of Biological Markers and Neuroimaging Methods for Prevention Trials Across all Stages

and Target Populations", The -journal of prevention of Alzheimer's disease, 1(3), pp. 181-202, 2014.

[11] "Sleep, Learning, and Memory | Healthy Sleep", Healthysleep.med.harvard.edu, 2017. [Online]. Available: http://healthysleep.med.harvard.edu/healthy/matters/benefits-of-sleep/learning-memory.

[12] S. Dubovik, R. Ptak, T. Aboulafia, C. Magnin, N. Gillabert, L. Allet, J. Pignat, A. Schnider and A. Guggisberg, "EEG Alpha Band Synchrony Predicts Cognitive and Motor Performance in Patients with Ischemic Stroke", Behavioural Neurology, vol. 26, no. 3, pp. 187-189, 2013.

[13] H. Berger, "Über das Elektrenkephalogramm des Menschen", Archiv für Psychiatrie und Nervenkrankheiten, vol. 87, no. 1, pp. 527-570, 1929.

[14] M. Bell, "Power changes in infant EEG frequency bands during a spatial working memory task", Psychophysiology, vol. 39, no. 4, pp. 450-458, 2002.

[15] G. Pfurtscheller and F. Lopes da Silva, "Event-related EEG/MEG synchronization and desynchronization: basic principles", Clinical Neurophysiology, vol. 110, no. 11, pp. 1842-1857, 1999.

[16] C. Babiloni, F. Carducci, F. Cincotti, P. Rossini, C. Neuper, G. Pfurtscheller and F. Babiloni, "Human Movement-Related Potentials vs Desynchronization of EEG Alpha Rhythm: A High-Resolution EEG Study", NeuroImage, vol. 10, no. 6, pp. 658-665, 1999.

[17] A. Bollimunta, Y. Chen, C. Schroeder and M. Ding, "Neuronal Mechanisms of Cortical Alpha Oscillations in Awake-Behaving Macaques", Journal of Neuroscience, vol. 28, no. 40, pp. 9976-9988, 2008.

[18] N. Crone, "Functional mapping of human sensorimotor cortex with electrocorticographic spectral analysis. I. Alpha and beta event- related desynchronization", Brain, vol. 121, no. 12, pp. 2271-2299, 1998.

[19] R. Acharya U., O. Faust, N. Kannathal, T. Chua and S. Laxminarayan, "Non-linear analysis of EEG signals at various sleep stages", Computer Methods and Programs in Biomedicine, vol. 80, no. 1, pp. 37-45, 2005.

[20] E. Niedermeyer and F. Lopes da Silva, Electroencephalography. Philadelphia: Lippincott Williams & Wilkins, 2005.

[21] R Buckner et al. "Opportunities and limitations of intrinsic functional connectivity MRI", Nature neuroscience, vol. 16, no. 7, pp. 832-837, 2013.

[22] "American Electroencephalographic Society Guidelines for Standard Electrode Position Nomenclature", Journal of Clinical Neurophysiology, vol. 8, no. 2, pp. 200- 202, 1991.

[23] A. Dale and M. Sereno, "Improved Localizadon of Cortical Activity by Combining EEG and MEG with MRI Cortical Surface Reconstruction: A Linear Approach", Journal of Cognitive Neuroscience, vol. 5, no. 2, pp. 162-176, 1993.

[24] B. Tóth, R. Boha, M. Pósfai, Z. Gaál, A. Kónya, C. Stam and M.Molnár, "EEG synchronization characteristics of functional connectivity and complex network properties of memory maintenancein the delta and theta frequency bands", International Journal of Psychophysiology, vol. 83, no. 3, pp. 399-402, 2012

[25] K. Mevel, G. Chételat, F. Eustache and B. Desgranges, "The Default Mode Network in Healthy Aging and Alzheimer's Disease", International Journal of Alzheimer's Disease, vol. 2011, pp. 1-9, 2011.

[26] N. Meziane, J. Webster, M. Attari and A. Nimunkar, "Dry electrodes for electrocardiography", Physiological Measurement, vol. 34, no. 9, pp. 47-69, 2013.

[27] M. Wenger, S. Negash, R. Petersen and L. Petersen, "Modeling and estimating recall processing capacity: Sensitivity and diagnostic utility in application to mild cognitive impairment", Journal of Mathematical Psychology, vol. 54, no. 1, pp. 73-89, 2010.

[28] H. Yuan, L. Ding, M. Zhu, V. Zotev, R. Phillips and J. Bodurka, "Reconstructing Large-Scale Brain Resting-State Networks from High-Resolution EEG: Spatial and Temporal Comparisons with fMRI", Brain Connectivity, vol. 6, no. 2, pp. 122-135, 2016.

[29] K. Celone, V. Calhoun, B. Dickerson, A. Atri, E. Chua, S. Miller, K. DePeau, D. Rentz, D. Selkoe, D. Blacker, M. Albert and R. Sperling, "Alterations in Memory Networks in Mild Cognitive Impairment and Alzheimer's Disease: An Independent Component Analysis", Journal of Neuroscience, vol. 26, no. 40, pp. 10222-10231, 2006.